What Sets the Strength of the Middepth Stratification and Overturning Circulation in Eddying Ocean Models?

CHRISTOPHER L. WOLFE AND PAOLA CESSI

Scripps Institution of Oceanography, University of California, San Diego, La Jolla, California

(Manuscript received 29 October 2009, in final form 15 January 2010)

ABSTRACT

The processes maintaining stratification in the oceanic middepth (between approximately 1000 and 3000 m) are explored using an eddy-resolving general circulation model composed of a two-hemisphere, semienclosed basin with a zonal reentrant channel in the southernmost eighth of the domain. The middepth region lies below the wind-driven main thermocline but above the diffusively driven abyssal ocean. Here, it is argued that middepth stratification is determined primarily in the model's Antarctic Circumpolar Current. Competition between mean and eddy overturning in the channel leads to steeper isotherms and thus deeper stratification throughout the basin than would exist without the channel. Isotherms that outcrop only in the channel are nearly horizontal in the semienclosed portion of the domain, whereas isotherms that also outcrop in the Northern Hemisphere deviate from horizontal and are accompanied by geostrophically balanced meridional transport. A northern source of deep water (water with temperatures in the range of those in the channel) leads to the formation of a thick middepth thermostad. Changes in wind forcing over the channel influence the stratification throughout the domain. Since the middepth stratification is controlled by adiabatic dynamics in the channel, it becomes independent of the interior diffusivity κ as $\kappa \to 0$. The meridional overturning circulation (MOC), as diagnosed by the mean meridional volume transport, also shows a tendency to become independent of κ as $\kappa \to 0$, whereas the MOC diagnosed by water mass transport shows a continuing dependence on κ as $\kappa \to 0$. A nonlocal scaling for MOC is developed that relates the strength of the northern MOC to the depth of isotherms in the southern channel. The results of this paper compare favorably to observations of large-scale neutral density in the World Ocean.

1. Introduction

The stratification in the upper subtropical ocean can be understood in terms of the ventilated thermocline theory, which shows that stratification can be maintained by a balance among vortex compression by the winds, the advection of planetary vorticity by the horizontal flow (Luyten et al. 1983), and potential vorticity homogenization (Rhines and Young 1982a,b). Additional stratification can be maintained at the base of the ventilated thermocline through a diffusive "internal" thermocline (Salmon 1990). Together, the ventilated, homogenized, and internal thermoclines constitute the main thermocline and occupy the top 300–700 m of the ocean in the subtropics (Samelson and Vallis 1997).

Efforts to explain the presence of stratification below the main thermocline can be traced to Munk (1966), which, together with Munk and Wunsch (1998), shows that the distribution of temperature, salt, and tracers in the abyss is consistent with an advective–diffusive balance with a diffusivity of 10^{-4} m^2 s^{-1}. While there is some evidence that basin-averaged diffusivities approach the value required by Munk and Wunsch in the abyss, below 3000 m (Polzin et al. 1997; Ledwell et al. 2000; Naviera Garabato et al. 2004), numerous measurements support the conclusion that diffusivities at middepth (between 1000 and 3000 m) are smaller than that required by a diffusive–advective balance by nearly a factor of 10 (Polzin et al. 1997; Kunze et al. 2006). Thus, there appears to be a slab of ocean 2000 m thick whose stratification cannot be explained either by local wind forcing or by diffusion.

Vallis (2000) argues that middepth stratification is due to the presence of water masses of different characteristics that are advected into the subtropics from their formation regions at high latitudes. He demonstrates that the presence of a zonal reentrant southern channel with a sill (analogous to Drake Passage in the Southern Ocean) is necessary for the formation of realistic abyssal stratification. This is

Corresponding author address: Christopher L. Wolfe, Scripps Institution of Oceanography, University of California, San Diego, 9500 Gilman Drive, La Jolla, CA 92093-0213.
E-mail: clwolfe@ucsd.edu

DOI: 10.1175/2010JPO4393.1

because dense water formed in or south of the channel can only spread northward below the depth of the sill since the reentrant channel cannot support the zonal pressure gradient required to balance geostrophic meridional flow.

This special character of the channel geometry also has consequences for the meridional overturning circulation (MOC) because, in the absence of eddies, any net upwelling due to Ekman suction in the channel must be compensated by southward flow at the depth of the sill. This provides a mechanism for dense water to be brought to the surface and transformed into lighter water without appealing to large interior diffusivities (Toggweiler and Samuels 1993, 1995, 1998).

The dynamics of the channel in the models of Vallis (2000) and Toggweiler and Samuels (1993, 1995, 1998) is laminar, in that the effects of mesoscale eddies are ignored. However, it has been demonstrated that the stratification in the channel is fundamentally controlled by eddy dynamics (e.g., Johnson and Bryden 1989; Karsten et al. 2002; Marshall and Radko 2003, 2006; Cessi and Fantini 2004; Cessi et al. 2006; Henning and Vallis 2005; Olbers and Visbeck 2005; Hallberg and Gnanadesikan 2006; Spence et al. 2009). In an eddying ocean, buoyancy and other tracers are transported by the residual flow, which is the sum of the mean and eddy flow. Unlike the mean flow, the residual flow is not constrained by geostrophy, so meridional transport can occur above the level of topography. This impacts the stratification in the channel and in the basin.

The idea that the Southern Ocean has a large influence on the MOC and middepth stratification has been explored using layer (Samelson 1999, 2004, 2009) and box (Gnanadesikan 1999; Johnson et al. 2007) models, as well as coarse-resolution general circulation models (Toggweiler and Samuels 1995, 1998; Klinger et al. 2003) and single-hemisphere eddy-resolving models (Henning and Vallis 2005). Although the layer and box models are useful for illustrating the mechanisms responsible for the formation of middepth stratification, their treatment of eddies is crude and motivated more by analytical simplicity than physical considerations. Further, by representing the abyss using only a few layers or boxes, much detail is lost and it is impossible to distinguish features such as abyssal thermoclines or thermostads. Coarse-resolution general circulation models bring more detail to the stratification, but their treatment of eddies requires parameterizations with poorly constrained coefficients. The eddy-resolving experiments of Henning and Vallis (2005) showed that nonzero middepth stratification throughout the basin can be maintained by eddy processes in the channel; however, the formation of middepth stratification is not the focus of their study, and they do not explore the effects of the northern boundary conditions on the middepth stratification.

In this article, we investigate the formation of middepth stratification and its response to changes in channel and basin geometry, surface forcing, and diffusivity. We attempt to address the following questions:

1) What is the effect of basin and channel geometry on the middepth stratification and MOC in an eddying ocean?
2) Is the response of an eddying ocean to changes in buoyancy and wind forcing different from that predicted by the laminar models?
3) To what extent does the middepth stratification depend on the value of the interior diapycnal diffusivity?

These questions are addressed with a series of experiments using an idealized eddy-resolving model in which the geometry, forcing, and diffusivity are varied. First, in section 2 we review some thermocline scaling theories, which are helpful in understanding the experiments. The eddy-resolving ocean model is described in section 3. The effects of geometry, buoyancy forcing, wind, and diffusivity on the model's middepth stratification are discussed in sections 4–7, respectively. In section 8, we discuss the scaling of the meridional overturning circulation with diffusivity, wind, and surface buoyancy forcing. The significance of these results is discussed in section 9, and concluding remarks are given in section 10.

2. Theory for the middepth stratification

In this section we show that the dynamics of a southern zonally reentrant channel [analogous to the Antarctic Circumpolar Current (ACC)] plays a fundamental role in determining the global middepth stratification. Figure 1 shows a schematic that illustrates the scales discussed in this section. For simplicity, we assume that buoyancy b depends only on temperature T, so that isotherms coincide with isopycnals. The relationship between buoyancy b and temperature T is $b = \alpha g T$, where α is the thermal expansion coefficient of seawater and g is the gravitational acceleration.

a. Channel stratification

For simplicity, consider a channel that extends to the ocean floor, as in Fig. 1. The channel cannot support zonal pressure gradients, and geostrophically balanced mean meridional flow is impossible. Any mean meridional flow must occur in frictional boundary layers near the surface and bottom. The sense of the meridional circulation is northward in the surface Ekman layer with a southward return flow in the bottom boundary layer. This circulation tends to overturn isopycnals. In the limit of a laminar ocean, the isopycnals in the channel would become vertical,

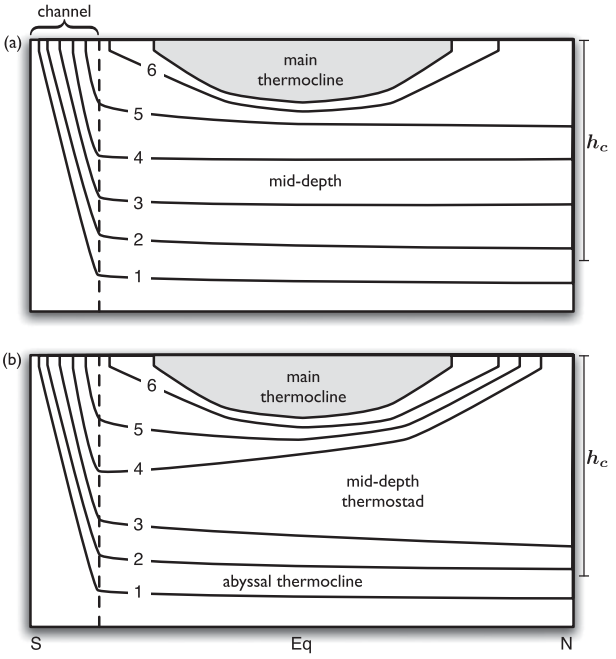

FIG. 1. Schematic illustrating the formation of deep stratification for the case of two hemispheres (a) without and (b) with a northern source of middepth water. Contours give isopycnals; contour labels are linear and monotonic and in arbitrary units.

with the wind-driven overturning balanced by convective mixing (e.g., Vallis 2000).

The available potential energy put into the overturning isopycnals by the wind is efficiently released at the mesoscale by baroclinic instability, leading to the formation of transient eddies. A scale depth for the stratification in the channel, h_c, can be derived in the limit of small diffusivity by assuming that overturning owing to the wind is balanced by interior eddy fluxes

$$\overline{w}\overline{b}_z \sim \nabla \cdot \overline{\mathbf{u}'b'}, \tag{1}$$

where an overbar denotes the temporal mean and a prime the deviation therefrom. The vertical velocity scales like the Ekman pumping, $\overline{w} \sim w_E \sim \tau_c/(\rho f_c L_c)$, where $\tau_c/(\rho f)$ is the surface Ekman transport in the channel, f_c is the Coriolis parameter at the channel edge, and L_c is the width of the channel.

A convenient way to encapsulate our ignorance of the eddy transport is to define an eddy diffusivity K_e that satisfies the flux gradient relationship

$$\overline{\mathbf{u}_h'b'} = -K_e \nabla_h \overline{b} \sim \frac{K_e \Delta b}{L_c}, \tag{2}$$

where the subscript h indicates the horizontal component and Δb is the range of surface buoyancy in the channel. If the interior eddy fluxes are adiabatic, then the horizontal and vertical components of the flux divergence have the same scale, so (1) implies that

$$h_c = \frac{\tau_c}{\rho f_c K_e} L_c. \tag{3}$$

Similar scalings for the channel stratification have been found by Karsten et al. (2002), Marshall and Radko (2003, 2006), Henning and Vallis (2005), Olbers and Visbeck (2005), and Cessi et al. (2006). Using $\tau_c/(\rho f_c) = 1\ \mathrm{m^2\ s^{-1}}$, $K_e = 1000\ \mathrm{m^2\ s^{-1}}$, and $L_c = 1000$ km gives $h_c = 1000$ m, which is significantly deeper than the scale depth of the main thermocline (~300 m for parameters appropriate to the numerical model). Unfortunately, this estimate is very sensitive to the value and spatial structure of K_e, and these are hard to estimate a priori. However, observations and the numerical results presented below both confirm the prediction that the isopycnal slopes are much steeper in the channel than in the enclosed part of the basin.

b. Stratification north of the channel

If the buoyancy forcing is such that the densest water formed in the Northern Hemisphere (NH) is lighter than any water formed in the channel, the middepth isopycnals will only outcrop in the channel. Provided interior diffusive upwelling is sufficiently weak that Stommel and Arons (1959) dynamics can be neglected, there will be no large-scale flow on these isotherms in the enclosed, basinlike part of the domain. Thus, these isotherms will be flat north of the channel.

Conversely, if the water formed in the NH has a density within the range of those found in the channel, the isopycnals less dense than the northern water must outcrop in the NH. This case is illustrated in Fig. 1b, where the northern water has a density between the isopycnals labeled 3 and 4, whereas isopycnals denser than the northern water need not be displaced. The parting of the two types of isopycnals will open a middepth thermostad that displaces less dense isotherms upward, sharpening the main thermocline. In this case, the stratification below the middepth thermostad is an isolated internal maximum of the stratification, reminiscent of the ''abyssal thermocline'' observed by Vallis (2000). Since the depths of the isopycnals at the northern edge of the channel are fixed by the dynamics of the channel, the middepth thermostad must get thinner toward the south.

The meridional pressure gradient, associated with isopycnals that have a meridional slope on a boundary, drives water down the pressure gradient in frictional boundary layers. The precise relationship between the meridional pressure gradient and the meridional transport depends on additional factors such as the interior circulation and

eddy fluxes of heat and potential vorticity near the boundary (see Cessi and Wolfe 2009). On isopycnals connected to the surface in both hemispheres, meridional transport can be maintained by differences in the subduction rates between the two hemispheres, leading to a pole-to-pole overturning circulation.

c. Consequences of the channel geometry

The view advanced in this section is that the middepth stratification is controlled by the stratification in the channel, especially on those isotherms that are ventilated only in the channel. This view has several testable consequences:

1) If the ocean basin is completely enclosed (i.e., there is no channel), middepth stratification will be very weak. Conversely, a basin with a channel should have stronger middepth stratification.
2) Isotherms that are ventilated only in the channel will be nearly horizontal.
3) A northern source of deep water (water with temperatures in the range of those in the channel) will lead to the formation of a middepth thermostad, pushing warmer isotherms upward.
4) Locally driven changes to the channel stratification should influence the stratification throughout the domain.

It is important to note that none of the above stratification mechanisms depend on the value of the interior diffusivity κ. Indeed, the mechanism for setting the stratification in the channel is explicitly adiabatic below the surface diabatic layer (Marshall and Radko 2003, 2006). We may thus expect that the abyssal stratification will become independent of the interior diffusivity as $\kappa \to 0$.

3. The eddy-resolving model

The eddy-resolving model used in the present experiments is similar to that used by Wolfe et al. (2008), Wolfe and Cessi (2009), and Cessi and Wolfe (2009). A brief description of the model is included here for completeness.

We employ the Massachusetts Institute of Technology General Circulation Model (MITgcm; Marshall et al. 1997a,b) to integrate the hydrostatic primitive equations in a simple flat-bottomed, rectangular domain with vertical sidewalls. Most of the experiments use the ''southern channel'' (SC) geometry shown in Fig. 2, which is an equatorially centered notched box with zonal extent $L_x = 2400$ km, meridional extent $L_y = 9800$ km, and depth $H = 2400$ m. The southernmost eighth of the domain is a zonally reentrant channel of extent $L_c = 1200$ km, analogous to Drake Passage latitudes of the Antarctic Circumpolar Current. The channel extends to the ocean bottom at $z = -H$. The ''no channel'' (NC) geometry is the same as the two-hemisphere SC geometry except that the channel is blocked. The ''south only'' (SO) geometry is the same as the Southern Hemisphere (SH) of the SC geometry, with a vertical no-slip wall at the equator.

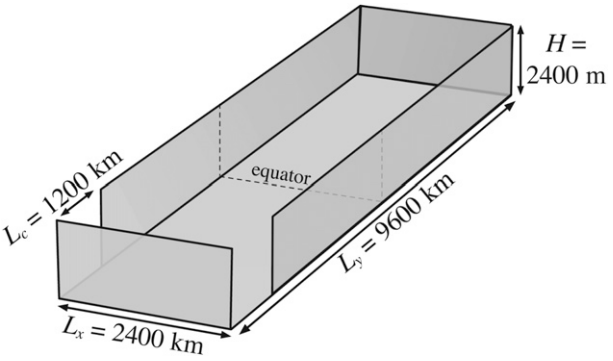

FIG. 2. Schematics of the southern-channel (SC) domain used in the most of the model simulations. The notch near the southern boundary is a zonal reentrant channel.

The momentum and thermodynamic equations are discretized on a fine Cartesian horizontal grid with a horizontal spacing of 5.4 km. The vertical grid has 20 levels with a stretched grid spacing that varies from 13 m at the surface to 274 m at the bottom. Consistent with the choice of a Cartesian grid, $f = \beta y$ with -4800 km $< y <$ 4800 km and $\beta = 2.3 \times 10^{-11}$ m^{-1} s^{-1}. Momentum is dissipated by horizontal Laplacian and biharmonic viscosity, vertical viscosity, and bottom drag with coefficients $A_h = 12$ m^2 s^{-1}, $A_4 = 9 \times 10^8$ m^4 s^{-1}, $A_v = 3 \times 10^{-3}$ m^2 s^{-1}, and $r = 4.1 \times 10^{-6}$ s^{-1}, respectively.

Buoyancy is a linear function of temperature only. Advective fluxes are calculated using either a third-order direct space–time scheme with a Sweby flux limiter (DST3) or a seventh-order monotonicity-preserving scheme (OS7MP). Both of these schemes avoid the generation of unphysical temperature extrema. The OS7MP scheme is less diffusive than the DST3 scheme, but was not implemented until some of experiments had been performed. Temperature is diffused via Laplacian diffusion with a constant, isotropic diffusivity κ. Surface buoyancy forcing is given by relaxation to a surface temperature distribution T_{surf} at the top grid point, with a relaxation time scale of 11 days. Convection is handled either by increasing the vertical diffusion to a large value (10 m^2 s^{-1}) in grid cells with unstable stratification (the IVD scheme) or directly via hydrostatic convection (the HC scheme). The results of the two schemes are very similar except that hydrostatic convection permits the existence of regions of negative stratification near the surface in the subpolar regions.

The parameters that are varied between the experiments are summarized in Table 1, and the surface forcing

TABLE 1. Configuration of the numerical experiments. The geometry codes NC, SO, and SC refer to the no-channel, south-only, and southern-channel geometries, respectively. See Fig. 3 for the profiles of the surface wind and buoyancy forcing. The advective-scheme codes OS7MP and DST3 refer to the seventh-order monotonicity-preserving and direct space–time schemes, respectively. The convection-scheme codes HC and IVD refer to the hydrostatic convection and implicit vertical diffusion, respectively.

Code	κ (10^{-4} m^2 s^{-1})	Geometry	Winds	Buoyancy forcing	Advection scheme	Convection scheme
NC	0.49	NC	Symmetric	CP	OS7MP	HC
SO	0.49	SO	Symmetric	CP	OS7MP	IVD
CP-k1	0.12	SC	Symmetric	CP	OS7MP	IVD
CP-k2	0.24	SC	Symmetric	CP	OS7MP	IVD
CP-k4	0.49	SC	Symmetric	CP	OS7MP	HC
CP-k8	0.98	SC	Symmetric	CP	DST3	HC
CP-Ws2	0.49	SC	South × 2	CP	OS7MP	HC
WP-k2	0.24	SC	Symmetric	WP	OS7MP	HC
WP-k4	0.49	SC	Symmetric	WP	OS7MP	HC
WP-k8	0.98	SC	Symmetric	WP	DST3	HC
WP-Ws2	0.49	SC	South × 2	WP	OS7MP	HC

functions are shown in Fig. 3. Figure 4 shows a snapshot of the vorticity at 100 m depth in the CP-k1 experiment. Away from the equatorial region, the domain is filled with eddies with scales ranging from 50 to 500 km. The eddy-free patch in the northwest corner of the domain has weak horizontal gradients in temperature. The large-scale vorticity features near $y = \pm 2250$ km are associated with inertial recirculation gyres in the western boundary current extensions.

4. The effect of geometry

In the experiment without a channel (NC) all of the stratification is compressed into the upper 500–600 m of the subtropics (Fig. 5a). The stratification below 1000 m is weak with the buoyancy frequency falling below 0.5×10^{-3} s^{-1} at 1500 m. Unlike the other experiments listed in Table 1, the temperature field in the NC experiment has not reached a statistically steady state below 1000 m and the sense of the temporal drift is toward weaker stratification. Thus, a fully equilibrated NC experiment will likely have even weaker stratification at middepth.

In the south-only experiment (SO), the isotherms tilt down strongly in the channel (Fig. 5b). They reach middepth at the northern edge of the channel and then become horizontal as they enter the enclosed part of the basin. Isotherms in the main thermocline are deflected downward owing to the strong wind-driven circulation in the subtropics. The coldest temperature contour (0.25°C) also deflects downward because of a weak, diffusively driven abyssal overturning cell below 1500 m. Between the main thermocline and the deep cell, however, the isotherms are remarkably horizontal.

The middepth stratification in the SO experiment is 2–3 times stronger than in the NC experiment (Fig. 6), confirming point 1 of section 2c: a basin with a channel has stronger middepth stratification than one without.

5. The effect of surface buoyancy forcing

If the northernmost temperature in a two-hemisphere basin is warmer than any of the channel temperatures, then the middepth isotherms only outcrop in the channel. As discussed in section 2c, these isotherms should remain horizontal and the addition of a second hemisphere should not lead to a significant change in middepth stratification. The numerical experiments bear out this expectation: the two-hemisphere case with a warm north pole (WP-k2, Fig. 7a) has very similar stratification at middepth to the south-only case (SO, Fig. 5b). The water mass formed by convection in the northernmost hemisphere is unable to pass beneath the main thermocline and remains trapped in the NH.

Conversely, if the northern temperature is within the range of the channel temperatures, the middepth isotherms outcrop both in the channel and in the NH. The water mass formed by convection in the NH is able to flow under the main thermocline and spread throughout the basin, forming a thick middepth thermostad (Fig. 7b). The stratification below the thermostad is slightly stronger than in the case with no thermostad owing to the downward displacement of isotherms colder than the thermostad (Fig. 8). The upward shift in the isotherms warmer than the thermostad leads to a sharpening of the main thermocline.

The strong meridional slope of the $T \geq 1$°C isotherms in the CP-k2 experiment suggests the presence of a strong western boundary current associated with the deep water. Figure 9 shows the transport Q between the 1° and 2°C isotherms for cases WP-k2 and CP-k2, defined as

$$Q(y) = \overline{\int_0^{L_x} \int_{\zeta(x,y,T_1,t)}^{\zeta(x,y,T_2,t)} v(x, y, z, t)\, dz\, dx}, \qquad (4)$$

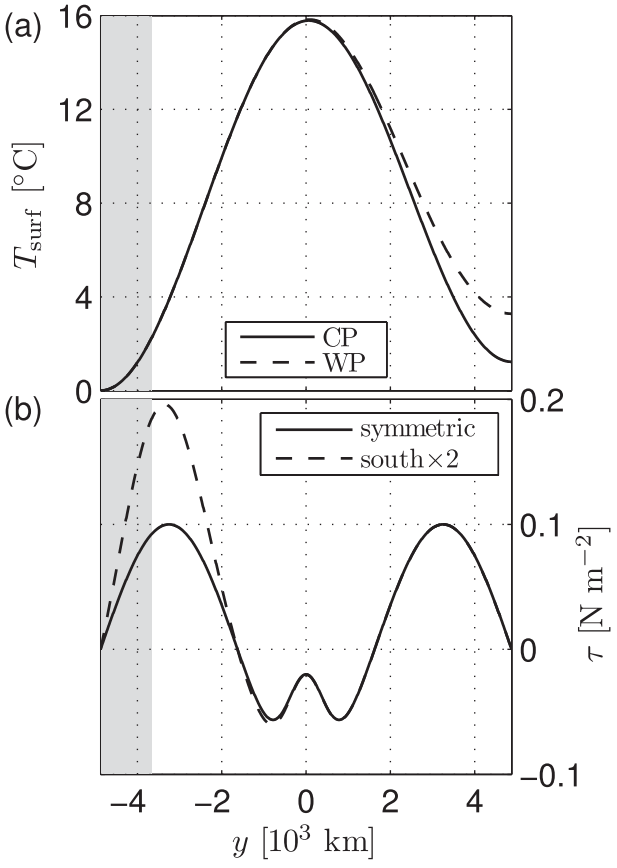

FIG. 3. Surface forcing functions for the experiments listed in Table 1: (a) surface relaxation temperature T_{surf} for the CP (solid) and WP (dashed) cases and (b) zonal wind stress τ for the "symmetric" (solid) and "south × 2" (dashed) cases. The shaded area is occupied by the reentrant channel in SO and SC cases. All forcing is zonally uniform. The meridional component of the wind stress is zero for all experiments.

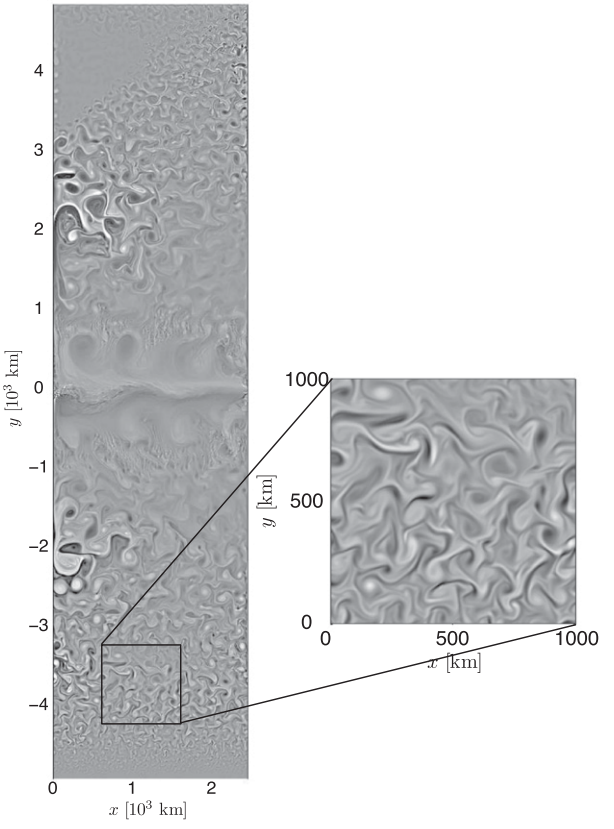

FIG. 4. Snapshot of vertical vorticity ζ at 100-m depth in the CP-k1 experiment. The maximum magnitude of ζ is 4×10^{-4} s^{-1} and is found in the western boundary current extensions. The grayscale ranges over $\pm 5 \times 10^{-5}$ s^{-1}. This shows detail in the ocean interior but oversaturates the western boundary extensions by almost a factor of 10. The inset shows detail in the channel.

where $T_1 = 1$°C, $T_2 = 2$°C, and $\zeta(x, y, \theta, t)$ is the height of the isotherm with temperature θ; that is, $T(x, y, \zeta(x, y, \theta, t), t) = \theta$. The CP-k2 experiment, in which the 1°–2°C isotherms outcrop in the NH as well as the channel, shows strong net southward transport in this temperature range, whereas the WP-k2 experiment has weak northward transport. This means that deep water is being transported southward from its formation region located in the northern subpolar gyre. The decline in deep-water transport as the water mass moves southward is due to diffusive transformation to warmer temperature classes.

There remains a small net transport of −0.4 Sv (Sv ≡ 10^6 m^3 s^{-1}) of deep water into the channel in the CP-k2 experiment. This transport is less than the −0.8 Sv due to Ekman suction between the 1° and 2°C outcrops because there is a convergence of surface eddy buoyancy fluxes into this water mass. The extrema in the channel are due to eddy transport of deep water southward through the outcrop of the 1°C isotherm and Ekman transport northward through the outcrop of the 2°C isotherm.

The northward transport in the WP-k2 experiment, shown in Fig. 9, is part of a diffusively driven abyssal cell that flows north from the channel, upwells through the 2°C isotherm, and returns to the channel near the surface in the SH.

6. The effect of Southern Ocean wind forcing

If the middepth stratification is controlled by the channel, local changes in the channel dynamics will impact the middepth buoyancy throughout the basin. Since the slope, $s = -b_y/b_z$, of the isotherms in the channel is determined by a balance between mean, wind-driven overturning and restratification by eddy fluxes, that is,

$$s \propto \frac{\tau_c}{\rho f_c K_e},$$

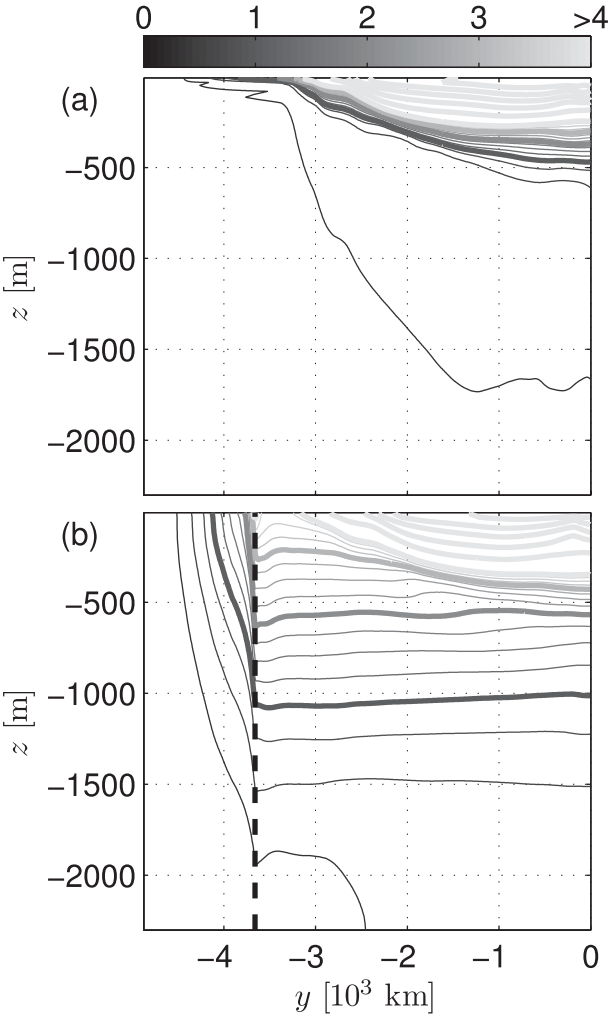

FIG. 5. Contours of temperature T (°C) along the western boundary for (a) the southern half of the experiment NC and (b) experiment SO: contour interval is 0.25°C for $T \leq 4°$ and 2°C for $T > 4$°C; integer valued contours are thick. The thick black line is $T = 1$°C. The northern boundary of the channel is shown by a vertical dashed line in (b).

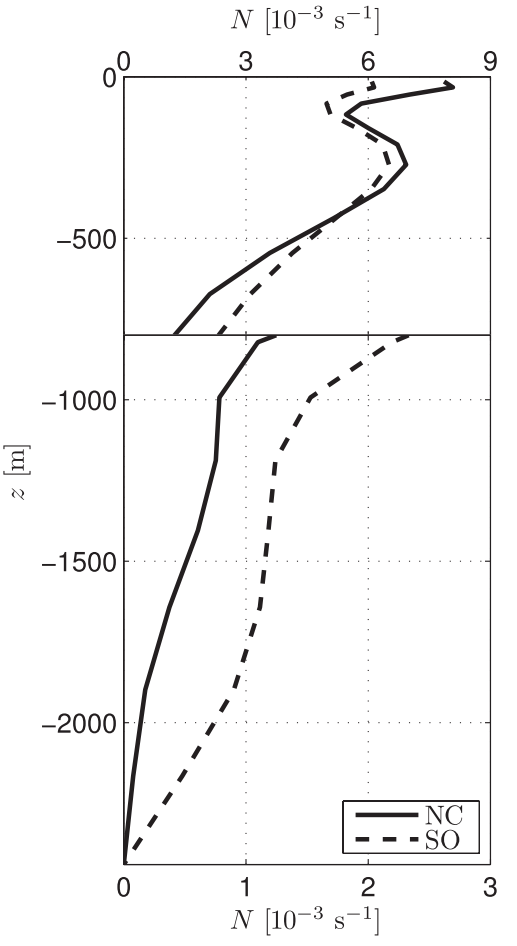

FIG. 6. Profiles of time-averaged buoyancy frequency $N = \sqrt{\overline{b}_z}$ in the southern subtropical gyre 600 km from the western boundary for the NC (solid) and SO (dashed) experiments. The scale of the abscissa has been expanded by a factor of 3 below 800 m to show detail in the abyss. The profile is averaged over time and a 60 km × 60 km horizontal area.

then a change in $\tau_c/(\rho f_c)$ over the channel will alter the isothermal slope, as long as eddy fluxes K_e do not completely compensate the effect of the wind (Marshall and Radko 2003, 2006).

We now discuss two experiments in which the wind is increased over the Southern Ocean, as shown by the dashed curve in Fig. 3b. This increased forcing is applied to experiments WP-k4, where middepth isotherms outcrop in the channel only, and CP-k4, where middepth isotherms also outcrop in the NH, yielding experiments WP-Ws2 and CP-Ws2, respectively. In both cases, the isothermal slope in the channel increases relative to the experiments with standard wind forcing (Fig. 10 shows experiments CP-k4 and CP-Ws2; the channel stratification of experiments WP-k4 and WP-Ws2 is very similar to that of experiments CP-k4 and CP-Ws2, respectively). The change in isothermal slope is not linearly proportional to the increase in wind forcing because the eddy diffusivity K_e increases with the slope.

The outcrop position of the isotherms is fixed by fast relaxation to the specified temperature distribution T_{surf}, so the increased slope results in a downward migration of isotherms at the northern edge of the channel. In response, the middepth isotherms are depressed throughout the basin north of the channel (Fig. 11). In both CP and WP series of experiments, isotherms that outcrop only in the channel shift downward 200–300 m. In the CP experiments, the depth of the isotherms that outcrop in both the channel and the NH increases by about 100 m.

In addition to driving changes in stratification, the increased wind forcing augments the transformation rate of

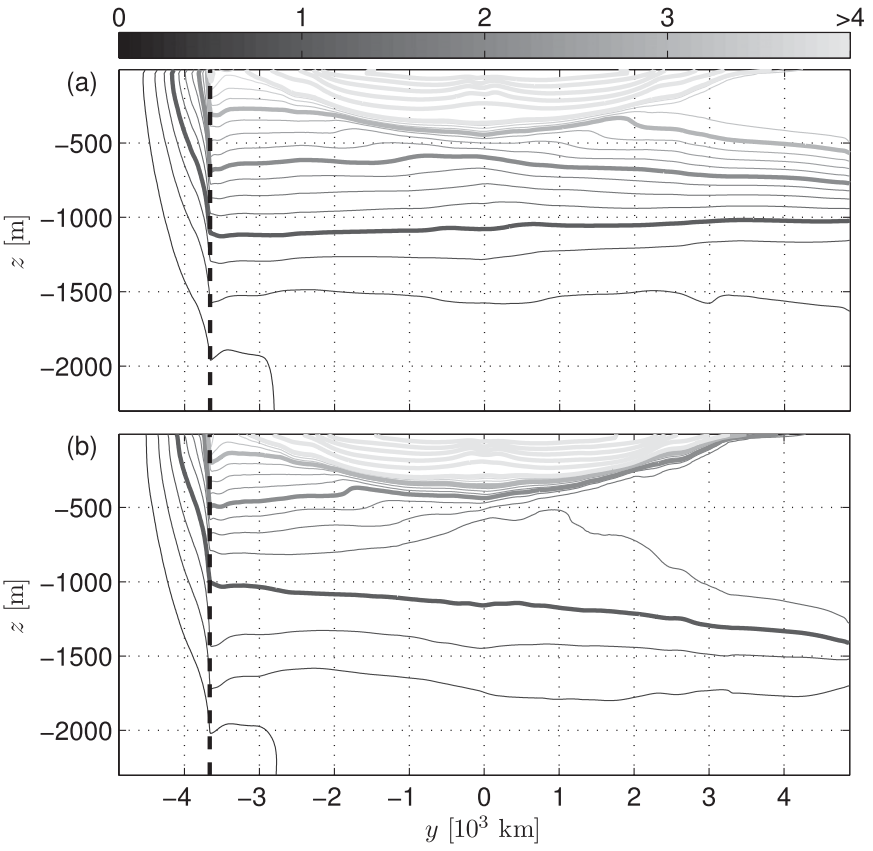

FIG. 7. As in Fig. 5 but for the (a) WP-k2 and (b) CP-k2 experiments.

water in the middepth temperature classes. The transformation occurs near the surface and is directly related to Ekman transport and the compensating horizontal eddy flux. For isotherms that outcrop in both hemispheres, a change in the water mass transformation in the channel is coupled to the water mass transformation in the NH and can lead to an increase in middepth water transport.

In the CP-Ws2 experiment, the surface eddy flux in the channel does not change significantly from the CP-k4 experiment. Thus, the difference in the water mass transformation rate between the two experiments is due to the change in the mean transport of water out of the deep water temperature class carried by the divergence of the Ekman flux. The change in transport is

$$\Delta Q \approx L_x[\Delta V_E(y_2) - \Delta V_E(y_1)] = \frac{L_x}{\rho}\left[\frac{\Delta\tau(y_2)}{f(y_2)} - \frac{\Delta\tau(y_1)}{f(y_1)}\right], \tag{5}$$

where V_E is the Ekman transport, $\Delta Q = Q_{\mathrm{CP-Ws2}} - Q_{\mathrm{CP-k4}}$, and $\Delta\tau$ is the difference in the wind stress; y_1 and y_2 are the outcrop positions of the 1° and 2°C isotherms, respectively. These outcrop positions are approximately the same in both experiments and have the values

$$y_1 = -4135 \text{ km} \quad \text{and} \quad y_2 = -3753 \text{ km}. \tag{6}$$

For the parameters used in experiments CP-Ws2 and CP-k4, $\Delta Q \approx -0.9$ Sv. This is very close to the observed change of -1 Sv in transport of deep water shown in Fig. 12. This change in transformation rate in the channel leads to a nearly meridionally uniform increase in the transport of deep water north of the channel and drives a corresponding increase in transformation in the NH.

Given that both experiments have the same forcing over the Northern Hemisphere, the results presented in this section demonstrate remarkable remote control of the NH ocean circulation by dynamics in the Southern Ocean and, in particular, in the channel for the CP cases.

7. The effect of diapycnal diffusivity

Classical theories of abyssal stratification (e.g., Munk 1966; Munk and Wunsch 1998) assume that abyssal dynamics is governed by a mean advective–diffusive balance.

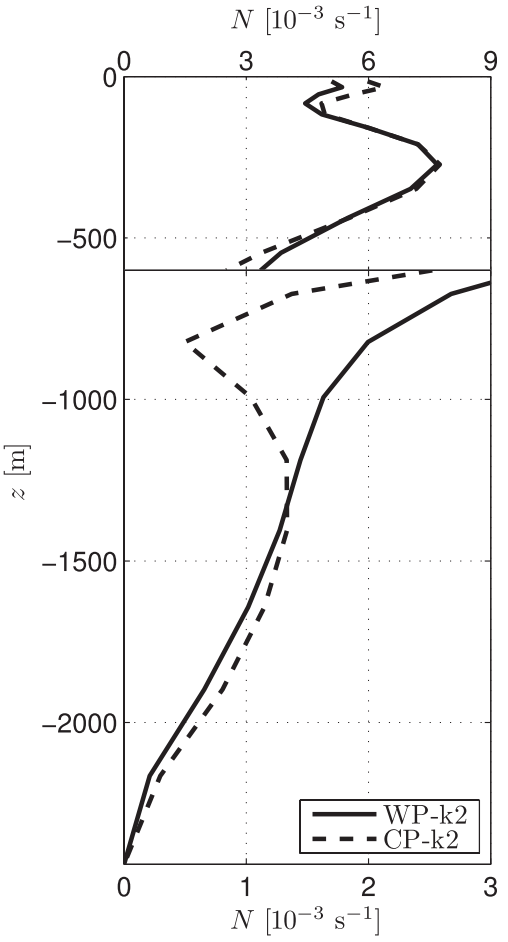

FIG. 8. Profiles of buoyancy frequency N in the northern subtropical gyre 600 km from the western boundary for the WP-k2 (solid) and CP-k2 (dashed) experiments. The scale of the abscissa has been expanded by a factor of 3 below 600 m to show detail in the abyss. The profile is averaged over a 60 km × 60 km horizontal area.

Although the particular scaling of the stratification with diffusivity will depend on the scale chosen for mean vertical velocity $\overline{w}$, one expects that, if such a balance holds, the stratification will tend monotonically to zero as $\kappa \to 0$.

In an eddying ocean model with a reentrant channel, there is the possibility of continuous middepth stratification in the limit of zero interior diffusivity. Since the eddies cause the channel isotherms to slump, the horizontal stratification across the surface of the channel is mapped continuously to vertical stratification at the northern edge of the channel (Wolfe and Cessi 2009). As shown in the previous sections, the stratification at the northern edge of the channel exerts a strong control on the stratification throughout the rest of the basin. Because the channel stratification is set adiabatically, the middepth stratification should become independent of κ as $\kappa \to 0$.

This prediction is tested by performing two sets of experiments in which the diffusivity κ is successively

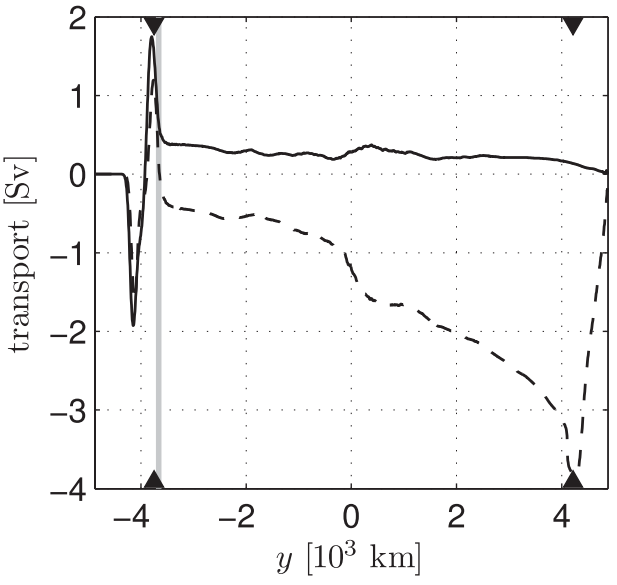

FIG. 9. Net meridional transport (Sv) between the 1° and 2°C isotherms for the WP-k2 (solid) and CP-k2 (dashed) experiments. The vertical gray line gives the position of the northern edge of the channel. The black triangles give the positions of the southern (WP-k2 and CP-k2) and northern (CP-k2 only) outcrops of the 2°C isotherm: that is, the meridional location where the 2°C isotherm intersects the surface at least 50% of the time.

halved or doubled from the base case with all other parameters held fixed. For the series (CP-k1, CP-k2, CP-k4, CP-k8), the middepth isotherms outcrop in the NH as well as in the channel. For the series (WP-k2, WP-k4, WP-k8), the deep water outcrops in the channel only. The profiles of the resulting buoyancy frequency N for these two sets of experiments are shown in Fig. 13. The profiles appear to be collapsing to a universal stratification as $\kappa \to 0$, especially in the middepth range $-1750 \text{ m} \le z \le 1000$ m. The middepth thermostad in the CP series becomes less stratified as $\kappa \to 0$. With the exception of the middepth thermostad, the magnitude and vertical structure of the stratification are very similar for the CP and WP series.

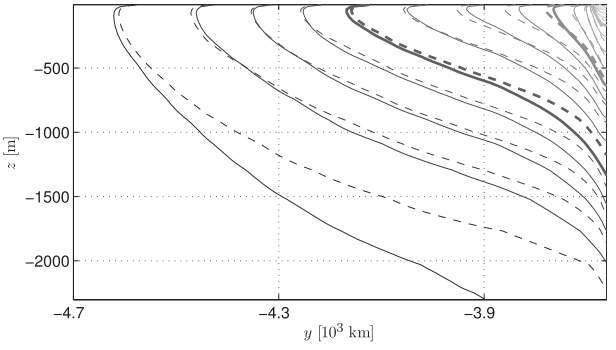

FIG. 10. Isotherms in the channel for the case with standard winds (CP-k4, dashed) and enhanced southern winds (CP-Ws2, solid).

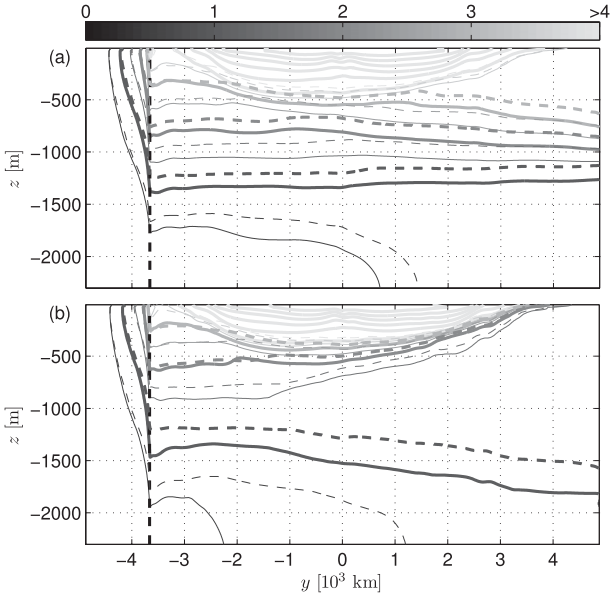

FIG. 11. Contours of temperature T along the western boundary in °C for (a) experiments WP-Ws2 (solid) and WP-k4 (dashed) and (b) experiments CP-Ws2 (solid) and CP-k4 (dashed): contour interval is 0.5°C for $T \leq 4°$ and 2°C for $T > 4$°C. The thick black line is $T = 1$°C. Integer valued contours are thick. Only isotherms for which $T \leq 4$°C are plotted for the WP-k4 and CP-k4 cases.

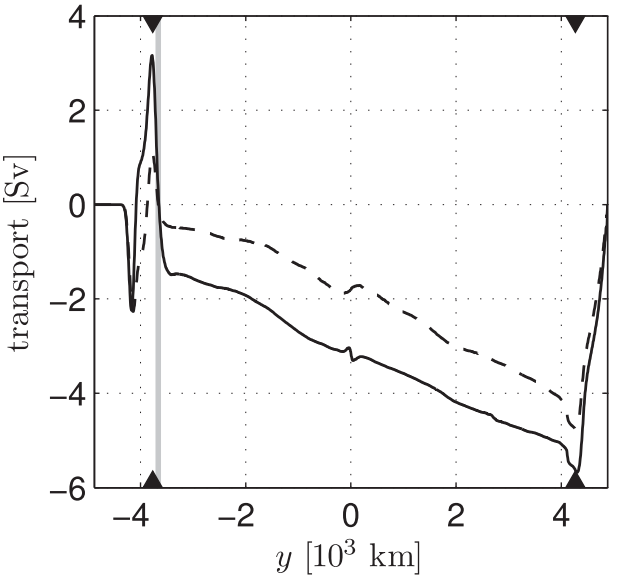

FIG. 12. As in Fig. 9 but for the CP-Ws2 (solid) and CP-k4 (dashed) experiments.

The transport Q of middepth water is shown in Fig. 14. Its meridional slope Q_y decreases with κ since the amount of middepth water lost to diffusive conversion into other density classes decreases with κ. In the limit $\kappa \to 0$, we expect that $Q_y \to 0$ where the middepth isotherms are not exposed to surface forcing and the MOC will comprise solely the pole-to-pole cell driven by interhemispheric differences in surface forcing.

Note that, in this section, we consider only the effect of the explicit interior diffusion and neglect the effects of numerical diffusion. As discussed in the appendix, we believe that the effects of numerical diffusion are small and do not significantly affect the results presented in this paper.

8. Meridional overturning circulation

a. Volume transport streamfunction

1) MODEL RESULTS

The meridional volume transport streamfunction ψ, which satisfies

$$\psi_z = -\int_0^{L_x} \overline{v}\, dx, \tag{7}$$

is a common diagnostic for the meridional overturning circulation. Figure 15 shows ψ for the CP-k1 experiment. The large magnitude of ψ above $z = -150$ m is due to wind-driven circulations in the ventilated thermocline and the equatorial region. Below these surface cells lies a pair of middepth cells with extrema at the latitudes of inertial recirculation gyres near the western boundary current extensions ($y \approx \pm 2250$ km). The northern cell, analogous to the Atlantic MOC, is stronger than the southern cell. The asymmetry of the middepth cells is due to a combination of the asymmetry in the surface buoyancy function (which would drive a stronger SH cell, see Fig. 3a) and a pole-to-pole cell driven by water mass transformation in the channel. There is evidence of a diffusively driven deep cell below $z = -1000$ m that is concentrated in the SH. The strong thermally indirect circulation in the channel is analogous to the Deacon cell in the Southern Ocean (Döös and Webb 1994).

2) SCALING OF THE MOC

(i) Scaling with diffusivity

The classical theories of the MOC hold that the overturning is driven by diffusive upwelling through the main thermocline. The strength of the overturning should then depend on some power of the diffusivity κ—in particular, the overturning rate $\psi \to 0$ as $\kappa \to 0$. If the thermocline is purely diffusive (i.e., wind forcing can be ignored), the thermodynamics, vorticity, and thermal-wind equations imply that $\psi \sim \kappa^{2/3}$. In the case of the wind-driven ventilated thermocline, the MOC is driven by diffusive upwelling through the internal thermocline located below the ventilated thermocline. The scale analysis proceeds as in the diffusive thermocline, but the depth

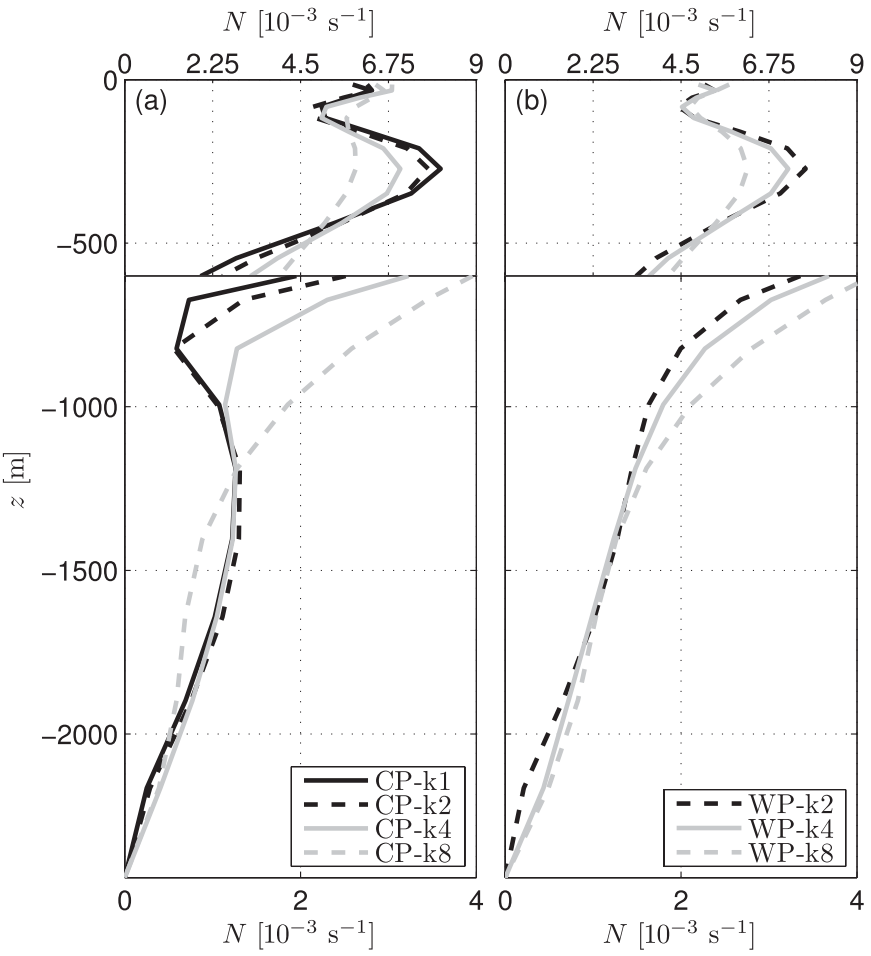

FIG. 13. As in Fig. 8 but for experiments (a) CP-k1, CP-k2, CP-k4, and CP-k8 and (b) WP-k2, WP-k4, and WP-k8.

scale used in the thermal wind equation is the depth of the ventilated thermocline, not the thickness of the internal thermocline. In this case, $\psi \sim \kappa^{1/2}$. [for a detailed discussion of the classical scalings for the MOC, see, e.g., Vallis (2006), section 16].

The northern subsurface maximum $\psi_{\max}$ of ψ is an indicator of the strength of the deep water overturning cell. At larger diffusivities ($\kappa > 4 \times 10^{-5}$ m^2 s^{-1}), $\psi_{\max}$ scales with the laminar scaling of the internal thermocline, $\psi_{\max} \propto \kappa^{1/2}$, for both CP and WP series of experiments (Fig. 16). The scaling becomes flatter as the diffusivity is reduced; the slope $\kappa^{1/5}$ is indicated in Fig. 16, but this is not significantly different from κ^0, given the small number of experiments at low diffusivity. The flattening of $\psi_{\max}$ as $\kappa \to 0$ is consistent with the idea that some part of the northern overturning is independent of diffusivity. It will be shown in section 8b(2) that a component of the MOC diagnosed by ψ is due to adiabatic circulation on tilting isotherms. This circulation involves vertical motion, thus contributing to ψ, but does not require any interior diabatic forcing. Additionally, a finite MOC as $\kappa \to 0$ can be maintained in the CP experiments through a pole-to-pole overturning cell driven by water mass transformation in the channel (Toggweiler and Samuels 1993, 1995, 1998).

It is important to note that the classic thermocline scaling theories discussed in this section are all local theories, in that the thermocline thickness and velocity scales are assumed to be determined by the locally imposed wind forcing and buoyancy distribution. If, as it appears to be the case in the present experiments, the global stratification is controlled by dynamics in the channel, the overturning circulation may be better described by a nonlocal scaling relationship. This possibility is explored in the next section.

(ii) Nonlocal MOC scaling

By the definition (7), a scaling for the volume transport streamfunction ψ is

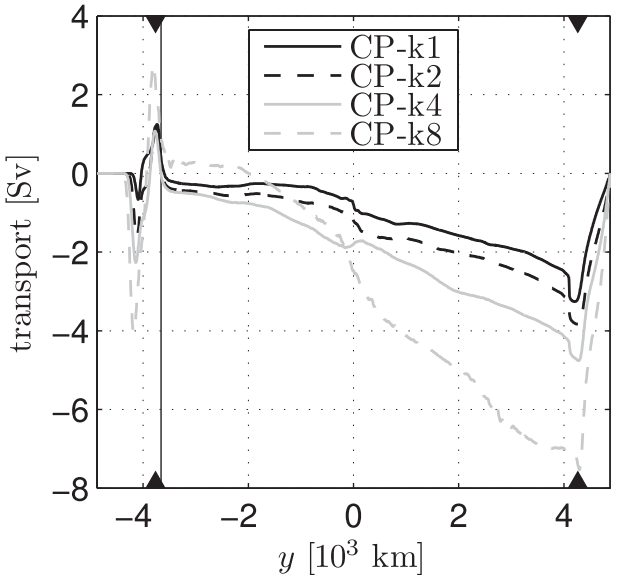

FIG. 14. As in Fig. 9 but for the CP-k1 (solid black), CP-k2 (dashed black), CP-k4 (solid gray), and CP-k8 (dashed black) experiments.

$$\psi \sim hL_x V, \tag{8}$$

where h is a scale for vertical variations of the streamfunction and V is a scale for the meridional velocity. Cessi and Wolfe (2009) showed that the large-scale meridional velocity below the wind-driven main thermocline is in thermal-wind balance with the large-scale zonal buoyancy gradient; that is,

$$V \sim h\frac{\Delta b_{\mathrm{EW}}}{fL_x}, \tag{9}$$

where $\Delta b_{\mathrm{EW}} = b(x = L_x) - b(x = 0)$ is the change in buoyancy from the east to the west coast. Thus, ψ obeys the scaling relationship

$$\psi \sim \frac{h^2 \Delta b_{\mathrm{EW}}}{f}. \tag{10}$$

These scales are evaluated at latitude of the subsurface maximum of ψ, approximately the boundary between the northern subtropical and subpolar gyres, where $w_{\mathrm{E}} = 0$.

To make this scaling relationship meaningful, we must determine scales for h and Δb_{EW}. As illustrated in Fig. 14, in the limit $\kappa \to 0$, the transport of middepth water between isopycnals that outcrop both in the Northern Hemisphere and in the channel, Δb_c, will be conserved along the lower branch of the pole-to-pole cell so that $h\Delta b_{\mathrm{EW}} = h_c \Delta b_c$. In the limit $\kappa \to 0$, the isopycnals that outcrop in the channel only will be horizontal in the enclosed part of the basins so that $h = h_c$, where

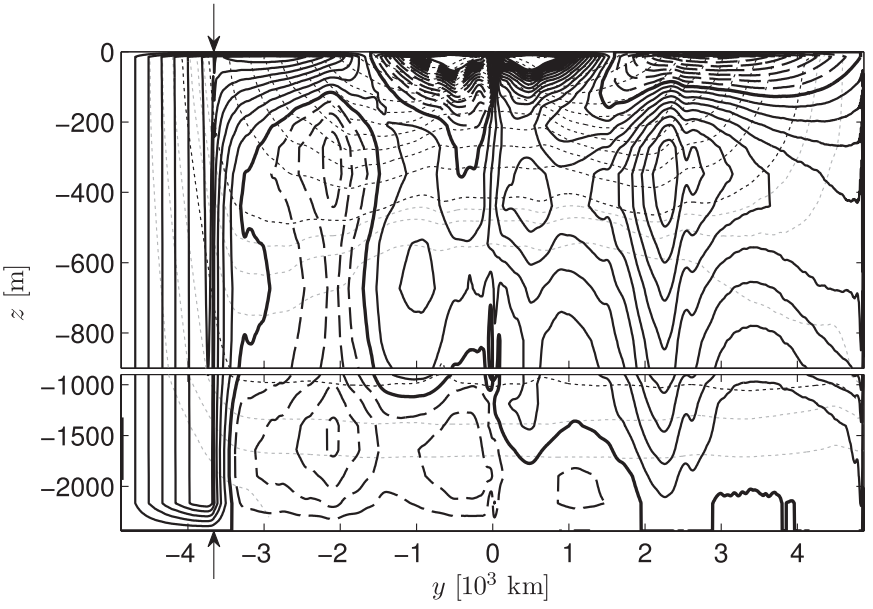

FIG. 15. The meridional overturning streamfunction ψ (Sv) for the CP-k1 experiment is shown with heavy contours: contour interval is 0.4 Sv; negative contours are dashed. Contours for $|\psi| > 6$ Sv are not plotted. Light, dotted contours give zonally averaged temperature with a contour interval of 0.25°C for gray contours and 1°C for black contours. The northern edge of the channel is indicated by inward-pointing arrows. Note the change in vertical scale in the lower panel.

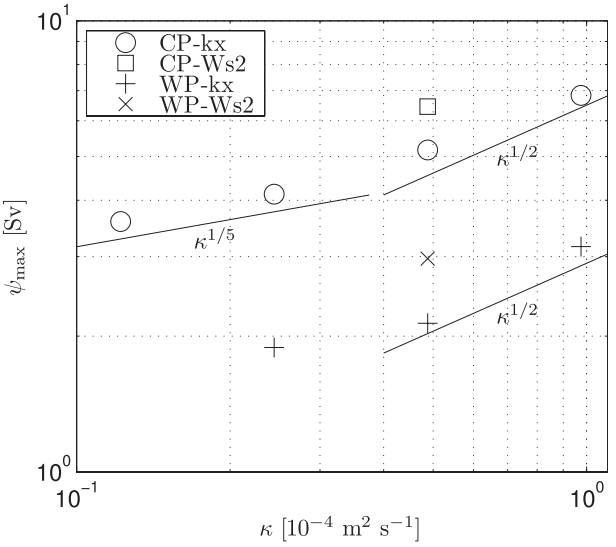

FIG. 16. Maximum middepth overturning rate $\psi_{\max}$ for the CP and WP series experiments as a function of diffusivity κ.

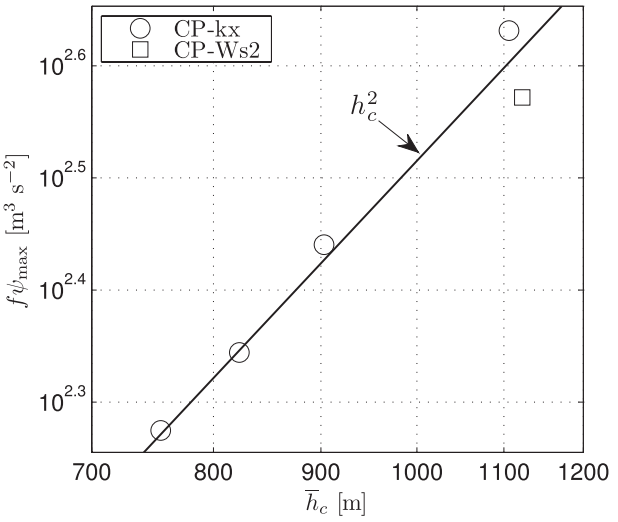

FIG. 17. The maximum northern overturning rate $\psi_{\max}$ multiplied by the Coriolis parameter f as a function of the streamwise-averaged depth $\overline{h}_c$ of the $T = T_{\text{surf}}(y_N)$ isotherm at the northern edge of the channel (circles). The line $f\psi_{\max} \sim h_c^2$ is shown for reference. Both axes are scaled logarithmically.

$$h_c \sim \frac{\tau_c}{\rho f_c K_e} l_c. \tag{11}$$

Here τ_c is the amplitude of the wind over the channel and l_c is the distance between the southern outcrop of the $T = T_{\text{surf}}(y_N)$ isotherm and the northern edge of the channel: that is, the distance encompassed by the range Δb_c.

The scaling for the MOC in the CP case, ψ_{CP}, is then

$$\psi_{\text{CP}} = \frac{h_c^2 \Delta b_c}{f} = \left(\frac{\tau_c l_c}{\rho f_c K_e}\right)^2 \frac{\Delta b_c}{f}. \tag{12}$$

What is special about this scaling is the choice of h and Δb that involve the remote scales of the channel stratification and the interhemispheric buoyancy difference. Note that this scaling predicts only the leading-order transport of the MOC in the limit $\kappa \to 0$. There are other contributions to the MOC due to diffusive processes. In the WP experiments, where $\Delta b_c = 0$, the term (12) vanishes and the MOC is diffusive to leading order.

The scaling (12) is incomplete without a scaling for K_e. As an alternative to determining a scaling for K_e, we can measure the streamwise-averaged depth $\overline{h}_c$ of the $T = T_{\text{surf}}(y_N)$ isotherm at the northern edge of the channel and use the expression after the first equality in (12). This will only test whether h_c is the appropriate vertical scale for the MOC; a test of the buoyancy scale Δb_c in (12) will require experiments with a larger range of the pole-to-pole temperature difference and is a subject of future work.

Here ψ_{CP} follows the scaling estimate $f\psi_{\max} \propto \overline{h}_c^2$ very closely (Fig. 17). The meridional position of the maximum of ψ varies sufficiently between the experiments that multiplication of $\psi_{\max}$ by f is essential to get the good fit in Fig. 17. There is no such scaling for the WP case: the stratification at the northern edge of the channel does not provide the relevant scale height for the MOC when no isopycnal connection exists between the NH and the channel.

It is interesting to note that $\overline{h}_c$ in the CP-Ws2 case is only 1.2 times that of the CP-k4 case, even though the wind stress over the channel is twice as strong in the former case than in the latter. The less than doubling of $\overline{h}_c$ as τ_c is doubled emphasizes the essential role of eddies in shaping the deep stratification.

b. Isopycnally averaged overturning streamfunction

1) FORMULATION

The advantages of diagnosing the MOC using ψ defined by (7) lie partially in its ease of calculation and interpretation. However, there is a strong temptation to regard the overturning cells revealed by ψ as representing actual diapycnal motion. This leads to the impression that the MOC diagnosed from ψ is closely related to the meridional heat flux. In fact, it is well known that many of the features of ψ are artifacts created by performing the temporal average and zonal integration at constant height (see, e.g., Döös and Webb 1994; McIntosh and McDougall 1996).

A streamfunction analogous to the residual streamfunction of transformed Eulerian mean (TEM) theory can be defined by taking the temporal mean and zonal integral at constant T:

$$\psi_{\rm res}(y,\theta) = -\overline{\int_0^{L_x}\int_{-H}^{\zeta(x,y,\theta,t)} v(x,y,z,t)\,dz\,dx}, \quad (13)$$

where $\zeta(x, y, \theta, t)$ is the height of the isotherm $T = \theta$ at the given position (x, y) and time t; ζ satisfies $T[x, y, \zeta(x, y, \theta, t), t] = \theta$ for all x, y, and t. For θ outside of the range of $T_{\rm min}(x, y, t) \le \theta \le T_{\rm max}(x, y, t)$, we adopt the convention:

$$\zeta(x,y,\theta,t) = \begin{cases} -H, & \theta < T_{\rm min}(x,y,t) \\ 0, & \theta > T_{\rm max}(x,y,t), \end{cases} \quad (14)$$

where, for every point x, y, t,

$$T_{\rm min}(x,y,t) = \min T(x,y,z,t), \quad -H \le z \le 0 \quad (15)$$

and

$$T_{\rm max}(x,y,t) = \max T(x,y,z,t), \quad -H \le z \le 0. \quad (16)$$

The residual streamfunction $\psi_{\rm res}$ is related to the isopycnal transport Q, defined in (4) by $Q(y) = \psi_{\rm res}(y, T_2) - \psi_{\rm res}(y, T_1)$, and $\psi_{\rm res}$ is computed in T coordinates but can be mapped back into geographical coordinates using, for each value of y and θ, the zonal and temporal mean height $\hat{z}$ of that isotherm; that is,

$$\hat{z}(y,\theta) = \overline{\langle \zeta(x,y,\theta,t)\rangle}, \quad (17)$$

where $\langle\cdots\rangle$ is the zonal mean.

For a given y, θ, and t the isotherm labeled by θ may outcrop at various zonal locations. Suppose, for simplicity, that the isotherm labeled by θ outcrops only once at the (time varying) location $x = x_0(t)$, that $\zeta(x, y, \theta, t) = 0$ for $x \le x_0(t)$, and that $\zeta(x, y, \theta, t) < 0$ for $x \le x_0(t)$. Thus, $\hat{z}(y,\theta) \equiv \overline{\langle \zeta(x,y,\theta,t)\rangle} < 0$ as there is a nonzero contribution to the zonal and temporal means of ζ. This means that the ocean surface is not necessarily located at $\hat{z} = 0$ and that isotherms with $\hat{z} < 0$ may outcrop at certain times and zonal positions.

A useful measure of the amount of contact an isotherm has with the surface is

$$\mathcal{S}(y,\theta) = \overline{\langle \mathcal{H}[-z_s - \zeta(x,y,\theta,t)]\rangle}, \quad (18)$$

where $\mathcal{H}(z)$ is the Heaviside step function and z_s is the thickness of the model's surface layer. Here $\langle \mathcal{H}[-z_s - \zeta(x, y, \theta, t)]\rangle$ is simply the fraction of the zonal mean that the isotherm labeled by θ is exposed to the surface, so $\mathcal{S}(y, \theta)$ is the fraction of the combined zonal and temporal mean that the isotherm labeled by θ is exposed to the surface; $\mathcal{S}$ can be shown to be equal to the cumulative distribution of surface temperature at a given y (Schneider 2005). Isotherms that, at a given y, never intersect the surface have $\mathcal{S}(y, \theta) = 0$, whereas $\mathcal{S}(y, \theta) = 1$ for any isotherm that lies entirely in the surface layer. The median outcrop latitude y_0 of the isotherm labeled by θ satisfies $\mathcal{S}(y_0, \theta) = 0.5$.

2) MODEL RESULTS

The extrema of the overturning streamfunction at $y = \pm 2250$ km and the Deacon cell are completely eliminated in this view of the MOC (cf. Figs. 15 and 18), indicating that these features represent adiabatic circulation on tilting isotherms. The deep water cell extends from a maximum near the northern boundary to the channel following the 1.25°–1.75°C isotherms. The meridional gradient of the middepth cell is due to diffusive upwelling through the 2°C isotherm, mostly in the subtropics. The diffusively driven bottom water cell ($\psi_{\rm res} < 0$ below the 1°C isotherm) is also more distinct and continuous in this representation.

Note that, although the maximum of the deep water cell appears to penetrate to 1000-m depth in Fig. 18, the associated diapycnal transport is driven across outcropping isotherms by a westward surface flow down a zonal temperature gradient. The isotherms in question all outcrop along the northern boundary but slope downward toward the west, so their zonal average depth is below the surface. Note also that the local minimum in $\psi_{\rm res}$ near the bottom in the channel is a real feature caused by transient eddies, which develop a diapycnal heat-flux component as they interact with the bottom.

The middepth maximum of $\psi_{\rm res}$ in the subtropics shows a somewhat more consistent power-law behavior than the maximum of ψ (Fig. 19), though there is still a tendency for the scaling to become shallower as the diffusivity is reduced. The WP series of experiments have very weak deep water overturning, which is best fit by a $\kappa^{2/3}$ power law consistent with diffusive overturning. The CP series appears to follow a $\kappa^{1/3}$ power law, which is not consistent with either the purely diffusive or wind-influenced diffusive scaling. Not surprisingly, the interhemispheric isopycnal connection with the channel provides an effective mechanical forcing to the system that results in larger heat transport in the CP case. However, we do not observe a finite limit as $\kappa \to 0$: this is to be expected in a system where diffusivity is decreased everywhere, including the near-surface region (i.e., there is no mixed layer). In such as setting, we cannot expect the residual circulation to become independent of κ as $\kappa \to 0$.

9. Discussion

a. Connection to other models

The present results generalize the ideas of Toggweiler and Samuels (1993, 1995, 1998) by including the effect of

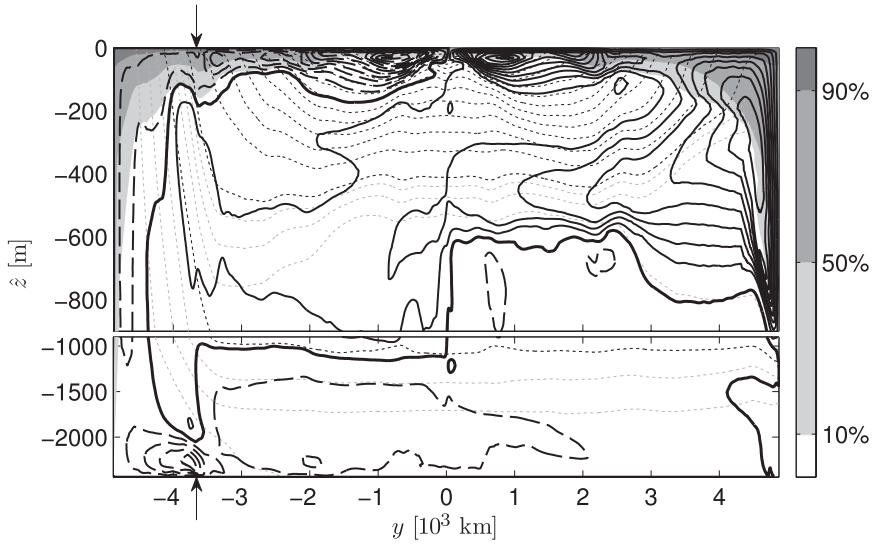

FIG. 18. The residual overturning streamfunction $\psi_{\rm res}$ for the CP-k1 experiment is shown with heavy contours. The abscissa is in nominal height coordinates $\hat{z}$: contour interval is 0.4 Sv; negative contours are dashed. Light, dotted contours give zonal and temporal mean isothermal height with a contour interval of 0.25°C for gray contours and 1°C for black contours. The shading shows the cumulative distribution of surface temperature $\mathcal{S}$. The northern edge of the channel is indicated by inward-pointing arrows. Note the change in vertical scale in the lower panel. Here $\psi_{\rm res}$ has been smoothed meridional by a Hanning filter with a half width of 33 km that operated along surfaces of constant T.

eddies. Eddies modify the Toggweiler and Samuels picture in two ways. First, since eddies cause the channel isotherms to slump, the importance of the sill is reduced: the depth of the middepth water mass is set by a competition between the mean and eddy flow and is not necessarily constrained by the depth of the sill. Second, we consider the residual circulation, which is generally not equal to the mean circulation. The residual circulation, not the volume circulation, is what transports buoyancy and, since it is not bound by the geostrophic constraint, net meridional buoyancy transport is possible at any depth. In the nearly adiabatic interior, the residual circulation is approximately conserved along isotherms (Marshall and Radko 2003, 2006), so the transport of middepth water is set by surface processes in the channel, consistent with Toggweiler and Samuels (1993, 1995, 1998). These surface processes include not only direct wind forcing but also significant horizontal diabatic eddy fluxes: about 50% of the poleward transport per unit degree of middepth water owing to the Ekman flow is cancelled by an eddy flux in the opposite direction.

The theory for the middepth stratification presented here is an elaboration of that put forth by Gnanadesikan (1999). Gnanadesikan's model is essentially a two-box model of the ocean with a box representing the middepth water mass and the other representing the main thermocline. This model is used as a basis for predicting the depth of the pycnocline D, taken by Gnanadesikan to be the interface between the two water masses on the western boundary. It is argued that D is set by competition among four effects: 1) transformation of light to dense water in the NH, 2) diffusive upwelling through the subtropical

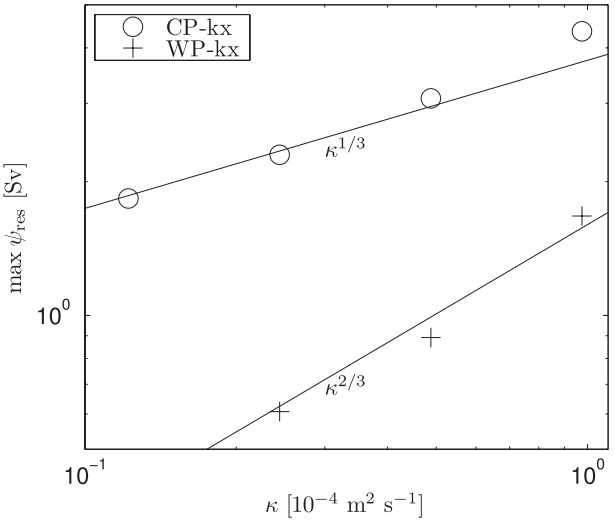

FIG. 19. Maximum middepth residual overturning rate $\psi_{\rm res}$ in the subtropics for the CP and WP series experiments as a function of diffusivity κ.

pycnocline, 3) equatorward transport of buoyancy by Southern Ocean winds, and 4) poleward transport of buoyancy by eddies in the Southern Ocean.

In the present work, the depth of the main thermocline appears to be fixed by dynamics local to the subtropics: the wind-driven ventilated thermocline and the eddy-diffusive internal thermocline. The depth of the main thermocline remains approximately constant throughout all of the experiments discussed here. In fact, the depth of the main thermocline is the same whether the channel is present or not (Fig. 6). This work attempts to explain the existence of stratification at middepth below the main thermocline but above the bottom water. The presence of continuous stratification at middepth for isotherms that do not outcrop in the NH argues against the appropriateness of a two-box model.

The depth of isotherms that do not outcrop in the NH appears to be controlled by the dynamics of the channel, and diffusion does not play a significant role: these isotherms spread horizontally equatorward of the channel and provide the basic deep stratification of our model ocean, without an associated overturn. Isotherms that outcrop in the NH can carry a net meridional transport as part of a pole-to-pole overturning cell. These isotherms have a zonal slope that results in deepening or shoaling on the western boundary. As in the analytical models of Samelson (1999, 2004, 2009), the zonal and meridional mean depth of these isotherms is strongly constrained by their depth at the northern edge of the channel, with diffusion a secondary effect.

According to the residual-mean theory of Marshall and Radko (2003, 2006), the channel stratification is determined by local processes in the limit of small residual circulation. All of the experiments listed in Table 1 have small residual circulations in the channel, so the communication between the channel and basin appears to be one way: the channel stratification controls the stratification in the basin, but the channel stratification is relatively insensitive to the Northern Hemisphere boundary conditions. Studies that have observed a large response of the channel to changes in conditions to the north (e.g., Fučkar and Vallis 2007) have large residual circulations in the channel. However, these studies employ eddy parameterizations that ignore the diabatic component of the eddy flux that results from the requirement that eddy motions become horizontal as the surface is approached (Ferrari et al. 2008). When surface diabatic eddy fluxes are accounted for (in the present study by fully resolving the eddies), the residual circulation is reduced for a given surface buoyancy flux due to cancelation with the diabatic eddy fluxes, and the sensitivity of the channel stratification to the conditions north of the channel is reduced.

b. Connection to observations

In the model ocean presented in this paper, the middepth stratification is strongly controlled by the channel and the dynamics of the channel can be understood in terms of the zonal-mean theory of Marshall and Radko (2003, 2006). This suggests that the middepth stratification of the World Ocean is similarly controlled by the dynamics of the Antarctic Circumpolar Current. One observational consequence of this control is that three major ocean basins connected to the ACC—the Atlantic, Indian, and Pacific—should have similar middepth stratification, to the extent that the ACC is along-stream homogeneous with respect to buoyancy.

Figure 20 shows the depth of three neutral density surfaces in the three major ocean basins. Neutral density γ_n is calculated using the method of Jackett and McDougall (1997) and data from the *World Ocean Atlas* (Locarnini et al. 2006; Antonov et al. 2006). The values of γ_n were chosen to have a roughly even vertical distribution between 1000 m (the bottom of the main thermocline) and 2500 m (the sill depth of the ACC). The middepth isoneutral surfaces in the Indian and Pacific Oceans outcrop only in the Southern Ocean; consequently, the depths of these isoneutral surfaces are nearly identical in these two basins. In contrast, the isoneutral surfaces in the Atlantic Ocean are systematically shallower than in the two other ocean basins as they outcrop in the Northern Hemisphere as well as in the ACC. According to the results of section 5, the Atlantic isoneutral surfaces are displaced upward to accommodate the water mass formed in the Northern Hemisphere (North Atlantic Deep Water). Even so, the depths of isoneutral surfaces, shown in Fig. 20, are approximately the same among all three basins at 40°S and vary by less than 20% elsewhere.

The similarity in the depths of the isoneutral surfaces between the ocean basins is especially remarkable considering that the ACC departs significantly from zonal symmetry. Apparently, these departures from zonally symmetry are not sufficient to significantly alter the basic dynamics of middepth stratification.

10. Summary

The scaling laws for middepth stratification, presented in section 2, have been examined using a series of experiments with an eddy-resolving general circulation model. We show that an ocean basin without a zonal reentrant channel has very weak middepth stratification. The addition of a channel leads to stronger middepth stratification because the wind-driven overturning circulation in the channel tends to make isotherms vertical and, despite competition by mesoscale eddies, steep buoyancy slopes are created.

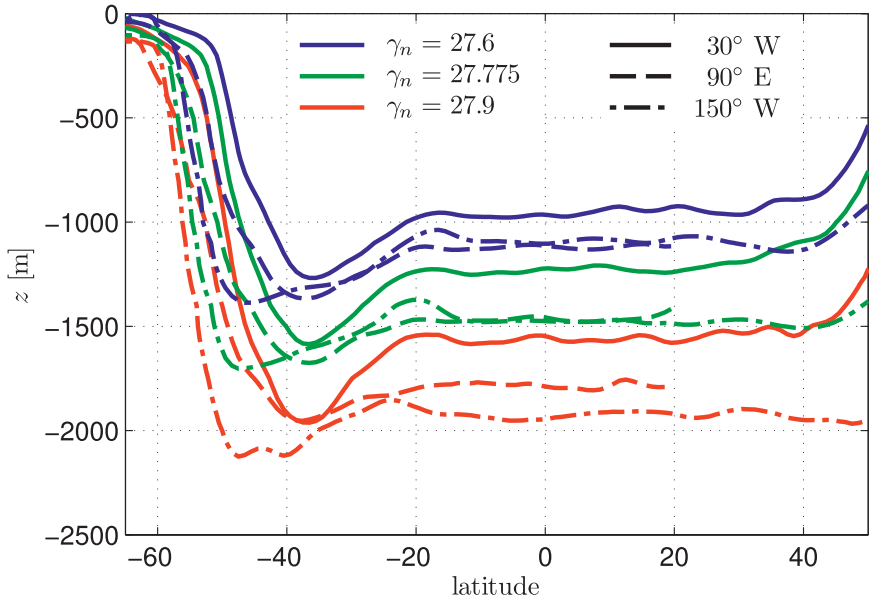

FIG. 20. Depth of three middepth neutral density γ_n surfaces as a function of latitude at three longitudes corresponding to the Atlantic (30°W), Indian (90°E), and Pacific (150°W) Oceans. Lines that are the same color represent the same value of γ_n, whereas lines that are the same style represent the same longitude.

The channel stratification strongly constrains the isopycnal geometry in the rest of the basin, and high buoyancy values achieve a deeper reach in the enclosed part of the basin than they would without the channel. Isopycnals that outcrop only in the channel remain horizontal in the basin portion of the domain. In contrast, isopycnals that outcrop in both hemispheres bend upward to outcrop in the NH, but their depths are still strongly constrained by the channel. These isopycnals allow a meridional pole-to-pole transport of water driven by interhemispheric differences in the transformation rate of water masses in the middepth density class. The water mass formed in the NH creates a middepth thermostad that pushes the warmer (colder) isotherms upward (downward). This leads to a sharpening of the main and abyssal thermoclines.

Because the middepth stratification is set by the channel, its dynamics influences middepth stratification throughout the domain. In particular, the slope of the isotherms in the channel increases if the wind over the channel is increased, leading to a downward migration of all the middepth isotherms in the NH subtropics.

The dynamics of the channel is nearly adiabatic beneath the surface layer. Consequently, the channel stratification, and thus the middepth stratification in general, does not depend strongly on the value of the interior diffusivity. In two series of experiments with different surface buoyancy forcing, profiles of buoyancy frequency become independent of the interior diffusivity as $\kappa \to 0$. We thus conclude that the middepth stratification is independent of κ.

The MOC as diagnosed using the mean meridional transport ψ appears to follow the wind-influenced $\kappa^{1/2}$ scaling for $\kappa > 4 \times 10^{-4}$ m^2 s^{-1}, but the scaling exponent becomes smaller as $\kappa \to 0$. This is consistent with the presence of adiabatic circulations on tilting isotherms near the western boundary current extensions and, in the CP experiments, a pole-to-pole overturning cell driven by water mass transformation in the channel. Both of these processes support a finite MOC as $\kappa \to 0$. In the CP experiments, the strength of the MOC is strongly coupled to the depth of the middepth isotherms at the northern edge of the channel, which in turn depends on the local wind stress. In particular, $f\psi_{\max} \sim \overline{h}_c^2 \Delta b_c$, where $\psi_{\max}$ is the subsurface maximum of the northern MOC, $\overline{h}_c$ is the streamwise-averaged depth at the northern edge of the channel of the isotherm with the same temperature as the northern boundary, and Δb_c is the range of buoyancies shared by the channel and the NH.

In the WP experiments, where $\Delta b_c = 0$, the channel dynamics is not implicated and the strength of the MOC is substantially less than in the CP cases. Nevertheless, the WP MOC is mechanically controlled by the winds in the SH: the volume transport in the NH increases as τ is increased in the southern subpolar region (cf. the x data point in Fig. 16). In both WP and CP cases, the remote mechanical forcing is an important driver of the NH volume transport, but we do not have an explicit scaling for the WP case.

The residual circulation ψ_{res} is another diagnostic for the MOC that is directly related to buoyancy transport.

When the northern temperature is warmer than any water found in the channel, the middepth cell is weak and follows a diffusive $\kappa^{2/3}$ scaling. When the northern temperature is in the range of those found in the channel, the middepth cell is stronger and follows a $\kappa^{1/3}$ scaling, for which we do not have an explanation. Further analysis is needed to understand the scaling of the residual circulation in this regime.

Acknowledgments. Our research is supported by the U.S. Department of Energy Office of Science (BER) Grant DE-FG02-01ER63252. Computational resources were provided by the Argonne Leadership Computing Facility and the National Center for Computational Sciences through INCITE, the National Energy Research Center through SciDAC, and the San Diego Supercomputer Center through the CyberInfrastructure Partnership.

APPENDIX

The Role of Numerical Diffusion

A nonlinear advection scheme is required to ensure that the temperature field remains bounded by its boundary and initial values in eddy-resolving z-coordinate models. A certain amount of numerical diffusivity is inevitable when using such a nonlinear advection scheme (Griffies et al. 2000).

We quantify the numerical mixing due to the advection scheme in the following manner. The buoyancy equation is written as

$$b_t + \nabla \cdot \mathbf{F} = \nabla_h \cdot \kappa \nabla_h b + (\kappa_v b_z)_z + Q, \qquad \text{(A1)}$$

where $\mathbf{F}$ is the buoyancy flux due to the nonlinear advection scheme, κ_v may include a contribution by the IVD convection scheme, and Q represents diabatic forcing at the surface. Multiplying (19) by b, time averaging, and integrating over the domain yields an entropy production budget:

$$\chi_d + \chi_a = \int \overline{bQ}\, dV \qquad \text{(A2)}$$

in which

$$\chi_d = \int \kappa \overline{|\nabla_h b|^2}\, dV + \int \overline{\kappa_v b_z^2}\, dV \qquad \text{(A3)}$$

and

$$\chi_a = -\int \overline{\nabla b \cdot \mathbf{F}}\, dV. \qquad \text{(A4)}$$

Numerical diffusion can be neglected if $|\chi_a| \ll \chi_d$. We find that this is the case for all of our experiments except for the one with the smallest diffusivity (CP-k1), where we still have $|\chi_a| < \chi_d$. Inspection of the integrand in (22) shows that $\overline{\nabla b \cdot \mathbf{F}} \le 0$ everywhere and the majority of the nonzero values are found in the upper tropical thermocline. Since surface tropical waters never directly interact with the middepth water masses, we believe that the relative insensitivity of the middepth stratification and overturning rate to κ as $\kappa \to 0$ is a real physical effect and not due to numerical diffusion.

REFERENCES

Antonov, J. I., R. A. Locarnini, T. P. Boyer, A. V. Mishonov, and H. E. Garcia, 2006: *Salinity*. Vol. 2, *World Ocean Atlas 2005,* NOAA Atlas NESDIS 62, 182 pp.

Cessi, P., and M. Fantini, 2004: The eddy-driven thermocline. *J. Phys. Oceanogr.,* **34,** 2642–2658.

——, and C. L. Wolfe, 2009: Eddy-driven buoyancy gradients on eastern boundaries and their role in the thermocline. *J. Phys. Oceanogr.,* **39,** 1595–1614.

——, W. R. Young, and J. A. Polton, 2006: Control of large-scale heat transport by small-scale mixing. *J. Phys. Oceanogr.,* **36,** 1877–1894.

Döös, K., and D. J. Webb, 1994: The Deacon cell and the other meridional cells of the Southern Ocean. *J. Phys. Oceanogr.,* **24,** 429–442.

Ferrari, R., J. C. McWilliams, V. M. Canuto, and M. Dubovikov, 2008: Parameterization of eddy fluxes near oceanic boundaries. *J. Climate,* **21,** 2770–2789.

Fučkar, N. S., and G. K. Vallis, 2007: Interhemispheric influence of surface buoyancy conditions on a circumpolar current. *Geophys. Res. Lett.,* **34,** L14605, doi:10.1029/2007GL030379.

Gnanadesikan, A., 1999: A simple predictive model for the structure of the oceanic pycnocline. *Science,* **283,** 2077–2079.

Griffies, S. M., R. C. Pacanowski, and R. W. Hallberg, 2000: Spurious diapycnal mixing associated with advection in a z-coordinate ocean model. *Mon. Wea. Rev.,* **128,** 538–564.

Hallberg, R., and A. Gnanadesikan, 2006: The role of eddies in determining the structure and response of the wind-driven Southern Hemisphere overturning: Results from the Modeling Eddies in the Southern Ocean (MESO) project. *J. Phys. Oceanogr.,* **36,** 2232–2252.

Henning, C. C., and G. K. Vallis, 2005: The effects of mesoscale eddies on the stratification and transport of an ocean with a circumpolar channel. *J. Phys. Oceanogr.,* **35,** 880–896.

Jackett, D. R., and T. J. McDougall, 1997: A neutral density variable for the world's oceans. *J. Phys. Oceanogr.,* **27,** 237–263.

Johnson, G. C., and H. L. Bryden, 1989: On the size of the Antarctic Circumpolar Current. *Deep-Sea Res.,* **36,** 39–53.

Johnson, H. L., D. P. Marshall, and D. A. J. Sproson, 2007: Reconciling theories of a mechanically driven meridional overturning circulation with thermohaline forcing and multiple equilibria. *Climate Dyn.,* **29,** 821–836, doi:10.1007/s00382-007-0262-9.

Karsten, R. H., H. Jones, and J. Marshall, 2002: The role of eddy transfer in setting the stratification and transport of a circumpolar current. *J. Phys. Oceanogr.,* **32,** 39–54.

Klinger, B. A., S. Drijfhout, J. Marotzke, and J. R. Scott, 2003: Sensitivity of basinwide meridional overturning to diapycnal diffusion and remote wind forcing in an idealized Atlantic–Southern Ocean geometry. *J. Phys. Oceanogr.,* **33,** 249–266.

Kunze, E., E. Firing, J. M. Hummon, T. K. Chereskin, and A. M. Thurnherr, 2006: Global abyssal mixing inferred from lowered ADCP shear and CTD strain profiles. *J. Phys. Oceanogr.,* **36,** 1553–1576.

Ledwell, J. R., E. T. Montgomery, K. L. Polzin, L. C. St. Laurent, R. W. Schmitt, and J. M. Toole, 2000: Evidence for enhanced mixing over rough topography in the abyssal ocean. *Nature,* **403,** 179–182.

Locarnini, R. A., A. V. Mishonov, J. I. Antonov, T. P. Boyer, and H. E. Garcia, 2006: *Temperature*. Vol. 1, *World Ocean Atlas 2005,* NOAA Atlas NESDIS 61, 182 pp.

Luyten, J., J. Pedlosky, and H. Stommel, 1983: The ventilated thermocline. *J. Phys. Oceanogr.,* **13,** 292–309.

Marshall, J., and T. Radko, 2003: Residual-mean solutions for the Antarctic Circumpolar Current and its associated overturning circulation. *J. Phys. Oceanogr.,* **33,** 2341–2354.

——, and ——, 2006: A model of the upper branch of the meridional overturning of the Southern Ocean. *Prog. Oceanogr.,* **70,** 331–345.

——, A. Adcroft, C. Hill, L. Perelman, and C. Heisey, 1997a: A finite-volume, incompressible Navier Stokes model for studies of the ocean on parallel computers. *J. Geophys. Res.,* **102,** 5753–5766.

——, C. Hill, L. Perelman, and A. Adcroft, 1997b: Hydrostatic, quasi-hydrostatic, and nonhydrostatic ocean modeling. *J. Geophys. Res.,* **102,** 5733–5752.

McIntosh, P. C., and T. J. McDougall, 1996: Isopycnal averaging and the residual mean circulation. *J. Phys. Oceanogr.,* **26,** 1655–1660.

Munk, W. H., 1966: Abyssal recipes. *Deep-Sea Res.,* **13,** 707–730.

——, and C. Wunsch, 1998: Abyssal recipes II: Energetics of tidal and wind mixing. *Deep Sea Res. I,* **45,** 1977–2010.

Naviera Garabato, A. C., K. L. Polzin, B. A. King, K. J. Heywood, and M. Visbeck, 2004: Widespread intense turbulent mixing in the Southern Ocean. *Science,* **303,** 210–213, doi:10.1126/science.1090929.

Olbers, D., and M. Visbeck, 2005: A model of the zonally averaged stratification and overturning in the Southern Ocean. *J. Phys. Oceanogr.,* **35,** 1190–1205.

Polzin, K. L., J. M. Toole, J. R. Ledwell, and R. W. Schmitt, 1997: Spatial variability of turbulent mixing in the abyssal ocean. *Science,* **276,** 93–96, doi:10.1126/science.276.5309.93.

Rhines, P. B., and W. R. Young, 1982a: A theory of wind-driven ocean circulation. I. Mid-ocean gyres. *J. Mar. Res.,* **40,** 559–596.

——, and ——, 1982b: Homogenization of potential vorticity in planetary gyres. *J. Fluid Mech.,* **122,** 347–367.

Salmon, R., 1990: The thermocline as an ''internal boundary layer.'' *J. Mar. Res.,* **48,** 437–469.

Samelson, R. M., 1999: Geostrophic circulation in a rectangular basin with a circumpolar connection. *J. Phys. Oceanogr.,* **29,** 3175–3184.

——, 2004: Simple mechanistic models of middepth meridional overturning. *J. Phys. Oceanogr.,* **34,** 2096–2103.

——, 2009: A simple dynamical model of the warm-water branch of the middepth meridional overturning cell. *J. Phys. Oceanogr.,* **39,** 1216–1230.

——, and G. K. Vallis, 1997: Large-scale circulation with small diapycnal diffusion: The two-thermocline limit. *J. Mar. Res.,* **55,** 223–275.

Schneider, T., 2005: Zonal momentum balance, potential vorticity dynamics, and mass fluxes on near-surface isentropes. *J. Atmos. Sci.,* **62,** 1884–1900.

Spence, P., O. A. Saenko, M. Eby, and A. J. Weaver, 2009: The Southern Ocean overturning: Parameterized versus permitted eddies. *J. Phys. Oceanogr.,* **39,** 1634–1651.

Stommel, H., and A. B. Arons, 1959: On the abyssal circulation of the world ocean—I. Stationary planetary flow patterns on a sphere. *Deep-Sea Res.,* **6,** 140–154.

Toggweiler, J. R., and B. Samuels, 1993: Is the magnitude of the deep outflow from the Atlantic Ocean actually governed by Southern Hemisphere winds? *The Global Carbon Cycle,* M. Heimann, Ed., NATO ASI Series, Vol. 15, Springer, 333–366.

——, and ——, 1995: Effect of Drake Passage on the global thermohaline circulation. *Deep-Sea Res. I,* **42,** 477–500.

——, and ——, 1998: On the ocean's large-scale circulation near the limit of no vertical mixing. *J. Phys. Oceanogr.,* **28,** 1832–1852.

Vallis, G. K., 2000: Large-scale circulation and production of stratification: Effects of wind, geometry, and diffusion. *J. Phys. Oceanogr.,* **30,** 933–954.

——, 2006: *Atmospheric and Oceanic Fluid Dynamics: Fundamentals and Large-Scale Circulation*. Cambridge University Press, 745 pp.

Wolfe, C. L., and P. Cessi, 2009: Overturning in an eddy-resolving model: The effect of the pole-to-pole temperature gradient. *J. Phys. Oceanogr.,* **39,** 125–142.

——, ——, J. L. McClean, and M. E. Maltrud, 2008: Vertical heat flux in eddying ocean models. *Geophys. Res. Lett.,* **35,** L23605, doi:10.1029/2008GL036138.